Dimension reduction by balanced truncation: Application to light-induced control of open quantum systems

Boris Schäfer-Bung,[1, a)] Carsten Hartmann,[1, b)] Burkhard Schmidt,[1, c)] and Christof Schütte[1, d)]
Institut für Mathematik, Freie Universität Berlin, Arnimallee 6, D-14195 Berlin, Germany.

(Dated: 8 June 2011)

In linear control, balanced truncation is known as a powerful technique to reduce the state-space dimension of a system. Its basic principle is to identify a subspace of jointly easily controllable and observable states and then to restrict the dynamics to this subspace without changing the overall response of the system. This work deals with a first application of balanced truncation to the control of open quantum systems which are modeled by the Liouville-von Neumann equation within the Lindblad formalism. Generalization of the linear theory have been proposed to cope with the bilinear terms arising from the coupling between the control field and the quantum system. As an example we choose the dissipative quantum dynamics of a particle in an asymmetric double well potential driven by an external control field, monitoring population transfer between the potential wells as a control target. The accuracy of dimension reduction is investigated by comparing the populations obtained for the truncated system versus those for the original system. The dimension of the model system can be reduced very efficiently where the degree of reduction depends on temperature and relaxation rate.

I. INTRODUCTION

Since the advent of suitable pulse shaping techniques in the 1980s, intense and short laser pulses have been used to control various quantum systems in physics and chemistry[1,2]. Starting from isolated atoms and molecules, the concept of laser control has been extended to condensed phases and biological systems[3,4]. Moreover, tailored laser pulses have also been applied to the control of chemical reaction dynamics thus opening the field of femtochemistry[5–10]. In all these fields, the light-induced control aims at driving a quantum system from an initial to a final (target) state both with high quantum yield and with high state specificity. In theoretical investigations, these targets are modelled by optimal control theory (OCT) employing forward and backward propagations iteratively in order to connect initial and final state, most often with the constraint of limited pulse fluence[11–15].

The main obstacle for the control of quantum many body systems is the exponential rise of the number of quantum states under consideration as a function of the number of the relevant degrees of freedom. This often leads to prohibitively long computing time and too large memory allocation because the numerical effort to solve the time-dependent Schrödinger equation (TDSE) is proportional to the number of quantum states involved. The problem is even more complicated if open quantum systems are to be modeled where an approximate treatment of (i) the influence of the environment (e. g. coupling to a heat bath) and/or (ii) dynamics of non-equilibrium systems have to be considered. In that case, the dynamics of a quantum system coupled to a bath can be described within the Markov approximation by the Liouville-von Neumann equation (LvNE) with a dissipative part in Lindblad form[16,17]. Since the number of entries of reduced matrices scales quadratically with the number of quantum states involved, propagations of these matrices are considerably more expensive than solving the TDSE for wave packet propagations.

A possible reduction of the effort could be obtained by the application of the multiconfiguration time-dependent Hartree method for density matrices (ρ-MCTDH)[18–20]. Systems like a Morse oscillator coupled to 60 harmonic bath oscillators[21] could be simulated successfully. However, this method is restricted to certain model Hamiltonians and certain limitations on the densities. The use of stochastic wave function methods is an alternative way to cope with high dimensionality[22–24] in density matrix propagation. However, the method is inefficient for non-local situations and the statistical error has to be compensated by averaging over a high number of realizations which is particularly problematic when rare events are to be treated[25]. In summary, there still is a strong need for the development of efficient methods for (reduced) density matrix propagation in order to progress toward higher dimensionality.

In the present work we shall explore possibilities for model reduction of the equations of motions (EOMs) for open quantum systems. The method of balanced truncation which stems from the field of engineering and was originally developed for systems with linear EOMs $\dot{x} = Ax + Bu$ where the external control field u is the input and the desired observable $y = Cx$ is the output. The balanced truncation method first maps states to certain linear combinations (called balanced states) which are ordered according to their ability to (a) react sensitively

a) boris.schaefer-bung@fu-berlin.de
b) chartman@mi.fu-berlin.de
c) Burkhard.Schmidt@fu-berlin.de
d) schuette@math.fu-berlin.de

on an external control field (input, controllability) and to (b) couple strongly to specified target states (output, observability) at the same time. Based on this transformation the balanced states are restricted to the subspace spanned by only those states which exceed a given threshold of controllability and observability. Hence, this truncation procedure guarantees that the input-output behaviour is approximately reproduced and that the remaining states can be safely neglected[26,27]. We would like to stress that in general this truncation scheme is not equivalent to truncation of energetically high lying states. For instance, there can be energetically low lying states, which are not observable due to too short life times and/or which are not controllable due to vanishing coupling moments. In addition to reducing the dimensionality, the balanced truncation method allows to keep the global approximation error under control[28,29], conserves the internal energy and equilibrium states[30], and can be generalized to positive systems[31] and Hamiltonian systems with friction[32]. Because model reduction can be understood as a projection onto a lower dimensional subspace which is *a priori* not unique, there are different variants of balanced truncation approaches: As an alternative to simple truncation (i.e., Galerkin projection) the restriction to the relevant subspace can also be realized by penalizing the hardly controllable and observable states. Penalization, which is more in the spirit of the singular perturbation approximation of balanced systems, has proven useful in preserving certain algebraic structures of the original system such as being Hamiltonian (see, e.g., Refs.[33,34]). As a rule of thumb, the singular perturbation approximation yields a good approximation of the low frequency modes in the system, whereas the Galerkin projection better captures the high-frequency behaviour[29].

It is noted that similar approaches to model reduction already exist: Krylov subspace methods are related to balanced truncation methods for linear and bilinear systems[35,36]. These iterative projection methods allow to calculate low rank approximations of the propagator by simple matrix-vector multiplications. Krylov methods are suitable for extremely high-dimensional systems ($n \approx 10^6$) and are frequently used for preconditioning. In contrast to balanced truncation, Krylov subspace methods are, however, in general not stability conserving and no error bound for the control of the approximation error can be given[37]. An alternative is the Hardy space (H_2)-approximation[38]. This method allows an optimal control of the approximation error by minimizing with respect to the H_2-norm. The basic variational principle can be augmented by algebraic boundary conditions that the reduced system conserves stability and positivity. However, the use of this nonlinear non-convex optimization routine is prohibitively expensive for high-dimensional systems.

The extension of balanced truncation to more complicated types of dynamics such as non-Markovian systems or systems with time-dependent coefficients is clearly possible. Typically this requires embedding of the system into a (considerably) higher-dimensional space in which the equations resume their simple form[39,40]. That is, though possible in general, such generalization are at the price of a much higher numerical effort, and for the sake clarity we refrain from considering these possibilities.

The goal of this article is to introduce the balanced truncation method into the field of control of open quantum systems and provide an efficient reduction of dimension. The LvNE with a dissipative part in Lindblad form is, however not of the linear structure mentioned above but contains a bilinear term for the coupling of the open quantum system to an external control field. Consequently, a generalization of the balanced truncation method beyond linearity is necessary. In a recent publication[41] we showed, that the dimensionality of a density evolution problem of the classical Fokker-Planck equation (applied to a dragged Brownian particle) can be efficiently reduced (to 2-5%) by the balanced truncation method generalized to bilinear systems $\dot{x}(t) = Ax(t) + u(t)Nx(t) + Bu(t)$ where structure and positivity are conserved. For open quantum systems the Liouville-von Neumann equation with a dissipative part in Lindblad form has to be rewritten as a bilinear equation, which exhibits the same structure.

This paper is organized as follows: In Section II we describe how we transform a dissipative LvNE to a bilinear form which is suitable for the balanced truncation method. In Section III the balanced truncation method is introduced and applied to an asymmetric double well model system in section IV. Results are discussed and summarized in Section V.

II. EVOLUTION OF OPEN QUANTUM SYSTEMS

An open quantum system can be described by the Liouville–von Neumann–equation[16,42]:

$$i\hbar\frac{\partial\hat{\rho}(t)}{\partial t} = \left[\hat{H}_0 - F(t)\hat{\mu}, \hat{\rho}(t)\right] + \mathcal{L}_D\left[\hat{\rho}\right], \qquad (1)$$

where the commutator on the rhs represents the closed system Liouvillian superoperator for the reduced density operator $\hat{\rho}$ containing the non-interacting system Hamiltonian $\hat{H}_0$ and the interaction with the external field $-\hat{\mu}F(t)$ composed in general by a j-fold product $F(t)$ of field tensors and the corresponding $(j-1)$-th order susceptibility $\hat{\mu}$ (e. g. electric dipole moment, polarizability). $\mathcal{L}_D$ is the open system Liouvillian in Lindblad form[43]

$$\mathcal{L}_D\left[\hat{\rho}\right] = i\hbar\sum_l\left(\hat{C}_l\hat{\rho}\hat{C}_l^\dagger - \frac{1}{2}\left[\hat{C}_l^\dagger\hat{C}_l, \hat{\rho}\right]_+\right), \qquad (2)$$

where l runs over all dissipation channels[23]. This functional in Lindblad form conserves the non-negativity of populations (i. e. the diagonal elements $\rho_{l,l}$ of the density matrix)[44]. The Lindblad operators $\hat{C}_l$ are composed of the dissipative transition rates $\Gamma_{k\to j}$ from the energy eigenstate $|k\rangle$ (with eigenvalue E_k) of $\hat{H}_0$ to the

state $|j\rangle$ (the set of eigenstates $\{|k\rangle, k = 0, \ldots, q-1\}$ is supposed to be finite) and a corresponding projection: $\hat{C}_l = \hat{C}_{j,k} = \sqrt{\Gamma_{k\to j}}\,|j\rangle\langle k|$. Energy relaxation, dephasing, and decoherence can be expressed in terms of these rates. A simple model for the treatment of dissipation is sketched in the following:

Considering anharmonicity in the system part, constant mass of the bath oscillators, and weak coupling limit, the downward relaxation rates can be determined by[45]:

$$\begin{aligned}\Gamma_{m\to n,m>n} = \quad & \frac{|\langle m|r|n\rangle|^2}{|\langle 1|r|0\rangle|^2}\cdot\frac{E_1-E_0}{E_m-E_n} \\ & \times\frac{1-\mathrm{e}^{-\frac{E_1-E_0}{k_BT}}}{1-\mathrm{e}^{-\frac{E_m-E_n}{k_BT}}}\cdot\Gamma_{1\to 0}\end{aligned} \tag{3}$$

The corresponding upward rates have to be calculated from detailed balance:

$$\Gamma_{n\to m,m>n} = \mathrm{e}^{-\frac{E_m-E_n}{k_BT}}\cdot\Gamma_{m\to n,m>n} \tag{4}$$

As can be seen in Eq. (3), in this model all transition rates depend on $\Gamma_{1\to 0}$. In the present work we understand $\Gamma_{1\to 0}$ as an adjustable parameter. Non-zero diagonal transition rates provide contributions to the dephasing and decoherence in the time evolution of the system. However, pure dephasing shall not be treated here which is the canonical choice.

The total dephasing rate can be determined by

$$\gamma_{l,m} := \frac{1}{2}\sum_{j=0}^{q-1}\Big(\Gamma_{l\to j}+\Gamma_{m\to j}\Big)\,. \tag{5}$$

Next we will show how the Liouville–von Neumann–equation (1) can be cast into a form applicable to the balanced truncation method. If we introduce the Bohr frequencies $\omega_{l,m} := (E_l - E_m)/\hbar$, and matrix elements: $\mu_{k,l} = \langle k|\hat{\mu}|l\rangle/\hbar$, in the energy eigenstate basis, Eq. (1) can be rewritten as[23]

$$\begin{aligned}\dot{\rho}_{l,m}(t) = & \Big(-i\omega_{l,m}-\gamma_{l,m}\Big)\rho_{l,m}(t)+\sum_{k=0}^{q-1}\Gamma_{k\to l}\rho_{k,k}(t)\delta_{l,m} \\ & + iF(t)\sum_{k=0}^{q-1}\Big(\mu_{l,k}\rho_{k,m}(t)-\rho_{l,k}(t)\mu_{k,m}\Big)\,.\end{aligned} \tag{6}$$

We now establish the relationship between the evolution equation (6), mean observables (8), and the bilinear input-output system consisting of the matrices A, N, B, and C[37,38,46]. The key point is vectorization of the density matrix[23,47]: i. e. the density matrix ρ of size q is mapped to a vector $x(\rho)$ with $n = q^2$ components. A detailed illustration for a two state model is given in Appendix A. Finally, Eq. (6) can be rewritten as:

$$\dot{x}(t) = Ax(t) + iF(t)Nx(t)\,, \quad x(0) = x_0\,. \tag{7}$$

In control theory, this equation is called input equation because it describes the dynamics of the system $x(t)$ depending on the (low dimensional) input field $F(t)$ and initial value $x(0) = x_0$.

In density matrix notation the expectation value $\langle O^{(j)}\rangle$ of the j-th observable $\hat{O}^{(j)}$ can be calculated as:

$$\langle O^{(j)}\rangle = \mathrm{Tr}\left\{\hat{O}^{(j)}\hat{\rho}\right\} = \sum_{k,l=0}^{q-1} O^{(j)}_{k,l}\rho_{l,k}\,. \tag{8}$$

In the context of control theory we are interested in the target of control which means we want to control the expectation values y:

$$y = \begin{pmatrix}\langle O^{(1)}\rangle \\ \langle O^{(2)}\rangle\end{pmatrix}, \tag{9}$$

the vectorization provides a shorthand notation of Eq. (8), see also Appendix A:

$$y(t) = Cx(t)\,, \tag{10}$$

where C is referred to as the observability matrix and the number m of observables (here $m = 2$), is typically small compared to the dimensionality n of the vectorized density matrix. Equation (10) is called the output equation because it represents the dynamics of the target.

In a second step the vectorized density x will be shifted: $x \mapsto \tilde{x} = x - x_e$, where $x_e = x(\rho_e)$ is the equilibrium density determined by the Boltzmann distribution

$$\rho^e_{k,k} = \mathrm{e}^{-\frac{E_k}{k_BT}}\left(\sum_{l=0}^{q-1}\mathrm{e}^{-\frac{E_l}{k_BT}}\right)^{-1}. \tag{11}$$

The shift ensures that controllability and observability conditions hold[48] for a system which is in equilibrium before field excitation. At the same time, x_e is the eigenvector of A corresponding to the eigenvalue 0 by virtue of (4) (i. e. $Ax_e = 0$). Hence, it follows:

$$\begin{aligned}&\dot{\tilde{x}}(t) = A\tilde{x}(t) + iF(t)N\tilde{x}(t) + iF(t)Nx_e\,, \quad \tilde{x}(0) = x_0 - x_e\,, \\ &\tilde{y}(t) = C\tilde{x}(t)\,, \quad \tilde{y}(t) = y(t) - Cx_e\,.\end{aligned} \tag{12}$$

Setting $B = Nx_e$ and renaming $u(t) = F(t)$ result in the desired bilinear (where $iu(t)Nx(t)$ is linear with respect to the field $u(t)$ and the density $x(t)$) input-output system derived from Eqs. (6) and (8), respectively:

$$\begin{aligned}&\dot{\tilde{x}}(t) = A\tilde{x}(t) + iu(t)N\tilde{x}(t) + iBu(t)\,, \quad \tilde{x}(0) = \tilde{x}_0\,. \\ &\tilde{y}(t) = C\tilde{x}(t)\,.\end{aligned} \tag{13}$$

On the one hand, the shift transforms a homogeneous equation to an inhomogeneous one and seems to complicate things. On the other hand, the shift establishes the basis for the balancing method described below in section III, by setting $x(0) = 0$ for an equilibrium starting condition. In the following we omit tildes to simplify notation.

III. BALANCED MODEL REDUCTION

Model order reduction is a branch of systems and control theory that aims at reducing the complexity of control systems, while preserving (as closely as possible) their input-output behaviour. It is better established for linear than for nonlinear systems and also the basic ideas and concepts can be most easily understood there, which is why we review linear systems first.

A. Linear systems

The simplest approximation to Eq. (13) is obtained by linearizing about the origin, $x = 0$, which results in a linear system of the form

$$\begin{aligned} \dot{x}(t) &= Ax(t) + iBu(t)\,, \quad x(0) = x_0\,, \\ y(t) &= Cx(t)\,. \end{aligned} \tag{14}$$

As before, the state vector $x \in \mathbb{C}^n$ represents the vectorized density matrix with the system matrix $A \in \mathbb{C}^{n\times n}$ containing differences of energy eigenvalues of H_0 and transition rates from $\mathcal{L}_D$ (see Eq. (A2) in Appendix A). The inhomogeneous part, Bu with the control matrix $B \in \mathbb{R}^{n\times p}$ and the control variable $u \in \mathbb{R}^p$ is meant to model a general time-dependent external field acting on the system; again the output vector $y \in \mathbb{R}^m$ describes the relevant observables in terms of the observability matrix $C \in \mathbb{R}^{m\times n}$. In almost any application of practical relevance, the state vector $x \in \mathbb{C}^n$ is very high-dimensional, even though u and y may be low-dimensional.[49] Therefore one wishes to reduce the dimensionality of the system while preserving the overall response of the observed quantities y to the external field u. Here the essential idea is to regard (14) as a map $u \mapsto y(u; x_0)$ that describes the observable y as a function of the control u (so-called transfer function).[50] The method of *balanced truncation* aims at keeping only those states that are most sensitive to the input field u (controllability) and, at the same time, strongly coupled to specified output states y (observability). Then, by construction, the remaining states hardly contribute to the transfer function of the system and therefore can be neglected.[26,27] In addition, balanced truncation allows for a global control of the approximation error by keeping or discarding as many states as desired.[28,29]

The concept of balanced truncation builds on the notion of *controllability and observability Gramian matrices*

$$\begin{aligned} W_c &= \int_0^\infty \mathrm{e}^{At} iB(-i)B^* \mathrm{e}^{A^* t}\mathrm{d}\,t\,, \\ W_o &= \int_0^\infty \mathrm{e}^{A^* t} C^* C \mathrm{e}^{At}\mathrm{d}\,t\,, \end{aligned} \tag{15}$$

that can be computed as the symmetric positive semidefinite solutions of the Lyapunov equations

$$AW_c + W_c A^* + BB^* = 0\,, \quad A^* W_o + W_o A + C^* C = 0\,. \tag{16}$$

Here and in the remainder of this chapter we assume that all eigenvalues of A have strictly negative real parts so that the integrals in (15) exist and are equal to the solutions of the Lyapunov equations.

Qualitatively, the controllability Gramian W_c is a measure for the control effort (in terms of the integral over $|u|^2$) that is needed to drive the system to a state x: given two states $x_1, x_2 \in \mathbb{C}^n$ with $|x_1| = |x_2|$, then x_1 can be reached with less control energy than x_2 if $x_1^* W_c x_1 > x_2^* W_c x_2$; in particular, if $W_c x_2 = 0$ then the state x_2 cannot be reached at all, regardless how strong the control field is; hence it cannot contribute to the transfer function of the system.

To see this, let $\xi \in \mathbb{C}^n$ an arbitrary vector and note that any admissible control that drives the system from the origin $x(0) = 0$ to a prescribed terminal state $x(t_f) = x_f$ must be of the form

$$u(s) = -iB^* \mathrm{e}^{A^*(t_f - s)}\xi \tag{17}$$

Together with the solution of (14)

$$x(t) = \int_0^t \mathrm{e}^{A(t-s)} iBu(s)\mathrm{d}\,s \tag{18}$$

for the initial value $x(0) = 0$, we find that

$$x(t_f) = \left(\int_0^{t_f} \mathrm{e}^{As} BB^* \mathrm{e}^{A^* s}\mathrm{d}\,s\right)\xi\,. \tag{19}$$

Calling the non negative matrix

$$W_c(t) = \int_0^t \mathrm{e}^{As} BB^* \mathrm{e}^{A^* s}\mathrm{d}\,s\,, \tag{20}$$

the finite time controllability Gramian, it readily follows that $x(t_f) = x_f$ can be reached if and only if

$$x_f = W_c(t_f)\xi \tag{21}$$

has a solution. If, moreover, the Hermitian matrix $W_c(t_f)$ is invertible, we can solve for $\xi = W_c^{-1}(t_f)x_f$. The corresponding control law

$$\hat{u}(s) = -iB^* \mathrm{e}^{A^*(t_f - s)} W_c^{-1}(t_f) x_f \tag{22}$$

then minimizes $\|u\|^2 = \int_0^{t_f} |u(s)|^2 \mathrm{d}\,s$ among all admissible controls $u \in L^2(0, t_f)$. The latter can be seen by the following simple calculation: for any admissible $u \in L^2(0, t_f)$ we have

$$\begin{aligned} \langle \hat{u}, u\rangle &= \int_0^{t_f} \hat{u}^*(s) u(s)\mathrm{d}\,s \\ &= \int_0^{t_f} ix_f^* \left(W_c^{-1}(t_f)\right)^* \mathrm{e}^{A(t_f - s)} Bu(s)\mathrm{d}\,s \\ &= x_f^* W_c^{-1}(t_f) x_f\,. \end{aligned} \tag{23}$$

Therefore, $\langle \hat{u}, u\rangle = \|\hat{u}\|^2$ which implies that

$$\|\hat{u}\|^2 = \|u\|^2 - \|u - \hat{u}\|^2\,. \tag{24}$$

Hence, $\hat{u}$ is the optimal control that minimizes $\|u\|^2$.

Conversely, the quadratic form $x^* W_o x$ with W_o being the observability Gramian measures how much "output energy" (i. e. the time integral over $|y|^2$) can be extracted from the system when $u = 0$ and the system has been initialized at $x(0) = x$; in particular, $W_o x = 0$ means that no output energy can be extracted; the state is then called *unobservable* and does not contribute to the transfer function.

Let us assume that (14) has neither unobservable nor uncontrollable states. Then, clearly W_c and W_o are positive definite, but it may still happen that some states are easier to control and observe than others; in particular there may be states that are hardly controllable or observable and we expect that they will not play such a big role for the system's transfer function. The very idea of *balancing* is to find a coordinate transformation $x \mapsto T^{-1}x$ under which controllability and observability Gramians become equal and diagonal, i.e.,[26,27]

$$T^{-1} W_c \left(T^{-1}\right)^* = T^* W_o T = \begin{pmatrix} \sigma_1 & & 0 \\ & \ddots & \\ 0 & & \sigma_n \end{pmatrix} = \Sigma \,. \quad (25)$$

The $\sigma_i > 0$ are *Hankel singular values* (HSVs) of the system. They are independent of the choice of coordinates as can be readily seen by noting that the squared HSVs are the eigenvalues of $W_c W_o$, namely,

$$T^{-1} W_c W_o T = \Sigma^2 \,.$$

The transformation T is a *contragredient transformation* and exists whenever W_c, W_o are symmetric and positive definite.[28] In the balanced representation, states that are least influenced by the input also have the least influence on the output and vice versa. Balanced truncation consists of first changing to the balanced coordinates, and then truncating the least controllable and observable states i. e. those states that have little effect on the transfer function.

A useful property of balanced truncation is that it admits easy control of the approximation error when truncating states. For example, we may obtain a reduced order system by projecting all the coefficients A, B, C onto the space spanned by the first $r < n$ columns of the inverse balancing transformation T. For the associated low-rank transfer function, $\hat{y}^{(r)} = \hat{y}^{(r)}(u; x_0 = 0)$, the following upper error bound holds[28]

$$\sup_{\|u\|_2=1} \|y(u;0) - \hat{y}^{(r)}(u;0)\|_2 < 2(\sigma_{r+1} + \ldots + \sigma_n)$$

where

$$\|w\|_2 = \int_0^\infty |w(t)|^2 dt \,.$$

Moreover *any* reduced order model of rank r satisfies the lower bound

$$\sup_{\|u\|_2=1} \|y(u;0) - \hat{y}^{(r)}(u;0)\|_2 \geq \sigma_{r+1}$$

which is typically close to the upper bound when the HSVs decay sufficiently fast. Note that also for time-dependent observability matrices $C(t)$[51] balanced truncation is applicable by an iterative procedure for the calculation of the observability Gramian. For example, a linear or quadratic time dependence of C(t) requires the solutions of three or five standard Lyapunov equations, respectively.

B. Bilinear systems

In contrast to the linear case, there is no comprehensive theory of model order reduction of bilinear systems (not to speak of general nonlinear systems)[48]. Especially quantitative statements such as computationally feasible upper or lower bounds for the approximation error are not available. For the sake of simplicity we consider bilinear systems of the form

$$\begin{aligned} \dot{x}(t) &= (A + iu(t)N)\, x(t) + iBu(t)\,, \quad x(0) = x_0 \\ y(t) &= Cx(t) \end{aligned} \quad (26)$$

having only a single input variabe $u \in \mathbb{R}$ (however, this is not a major restriction). Now recall the definitions (15)–(16) of the controllability and observability Gramians of the linear system (14). For bilinear systems, controllability and observability can be analyzed in terms of the generalized Gramians[52]

$$\begin{aligned} W_c &= \sum_{j=1}^{\infty} \int_0^\infty \ldots \int_0^\infty P_j(t_1, \ldots t_j) P_j^*(t_1, \ldots t_j) \mathrm{d}\, t_1 \ldots \mathrm{d}\, t_j \\ W_c &= \sum_{j=1}^{\infty} \int_0^\infty \ldots \int_0^\infty Q_j^*(t_1, \ldots t_j) Q_j(t_1, \ldots t_j) \mathrm{d}\, t_1 \ldots \mathrm{d}\, t_j \,, \end{aligned} \quad (27)$$

where we use the shorthand

$$\begin{aligned} P_1(t_1) &= \mathrm{e}^{At_1} iB\,, \quad P_j(t_1, \ldots, t_j) = \mathrm{e}^{At_j} iN P_{j-1} \\ Q_1(t_1) &= C\mathrm{e}^{A^* t_1}\,, \quad Q_j(t_1, \ldots, t_j) = Q_{j-1} iN \mathrm{e}^{A^* t_j} \,. \end{aligned} \quad (28)$$

Equivalently (provided that the above integrals exist) the generalized Gramians can be expressed by means of the generalized Lyapunov equations (cf. Eq. (16))

$$\begin{aligned} AW_c + W_c A^* + NW_c N^* + BB^* &= 0\,, \\ A^* W_o + W_o A + N^* W_o N + C^* C &= 0\,. \end{aligned} \quad (29)$$

Again, the uncontrollable or unobservable states are those states $x \in \mathbb{C}^n$ for which $W_c x = 0$ or $W_o x = 0$, respectively.[52] We argue along the lines of the linear case: Suppose again that controllability and observability Gramians are positive definite. We expect that the weakly controllable and observable states, i.e., these $x \in \mathbb{C}^n$ for which either $x^* W_c x$ or $x^* W_o x$ are small, do not contribute substantially to the input-output behaviour of the system and therefore can be discarded.[37] The assumption that the system is completely controllable and

observable is not essential and can be relaxed[53]. In this case the balancing transformation acts only on the susbpace of jointly controllable and observable states where the orthogonal complement that contains only states that are either uncontrollable, unobservable, or both uncontrollable and unobservable can be neglected (cf. also Ref. 49, Sec. 7.3). Under this assumption we may proceed as in the linear case: first transforming the system (26) to the balanced coordinates in which weakly controllable states coincide with weakly observable states and second truncating these states. As in the linear case, this second step is not unique and there are various options to truncate the system, depending also on the precise decay of the control term u as $t \to \infty$; we refer to our recent work for a discussion of the various possibilities.[41]

A detailed discussion of solvability and the numerical solution of the generalized Lyapunov equation is presented in Appendix B. If the solution of the generalized Lyapunov equation is too expensive or not feasible, principal component analysis (PCA) possibly represents an alternative to determine the Gramians which are necessary for the balanced truncation. A detailed derivation is shown in Appendix C.

IV. EXAMPLES

A. Model system

The balanced model reduction approach shall be applied to a dissipative quantum mechanical model system in density matrix formulation controlled by interaction with an external electric field. For simplification we consider one degree of freedom, s. The potential energy curve is chosen as an asymmetric double well represented by a fourth order polynomial:

$$H_0 = T + V(s) = -\frac{\hbar^2}{2I}\frac{\partial^2}{\partial s^2} + a_4(s^2 - d^2)^2 + a_1 s\,. \quad (30)$$

The model simulates e. g. conformational changes of molecules which can often be expressed as a function of one essential coordinate, or other types of molecular switches. We consider the asymmetric case in order (i) to get clearly localized wave functions in either well and (ii) to avoid tunneling between the potential wells.

The barrier height D is a characteristic quantity for the system. In the symmetric case ($a_1 = 0$) it is given by $D = V(0) - V(\pm d) = a_4 d^4$ and the two minima are separated in s-direction by $2d$. This almost holds for small asymmetry $a_1 d \ll D$, and $2a_1 d$ is the energy offset between both minima. We choose the parameters in Eq. (30) to $d = 1$, $a_4 = D$, $a_1 = 5.5 \cdot 10^{-2} D$, $I = 1.62 \cdot 10^2 \hbar^2 D^{-1}$ in order to obtain few levels in each well with maximal spacing. For a typical molecular application the barrier height for an inversion vibration is of the order of 10 kJmol^{-1} (≈ 0.1 eV) resulting in a moment of inertia of 5 uÅ^2, which is a typical value for a small molecule.

Numerical solution of the Schrödinger equation utilizing the Fourier grid method[54,55] provides the energy levels shown in Figure 1. It shows six vibrational levels in the left well and five levels in the right one where the maximal interlacing ($\omega_{1,0} \approx \omega_{2,0}/2$) of these levels minimizes tunneling and causes the high degree of localization of the corresponding energy eigenfunctions. In contrast, the energy eigenfunctions above the barrier are delocalized. We include ten additional levels up to twice the barrier height. Even in this system with only one degree of freedom fairly high dimensional matrices A, N, B, and C occur. The 21 considered states lead to a generalized tetradic representation of the density matrix (see Appendix A for details) with dimension n=441. Thus, reduction of the number of considered density matrix elements by balanced truncation is useful to accelerate dynamical simulations occuring, e. g. during a refinement of the control field in OCT simulations.

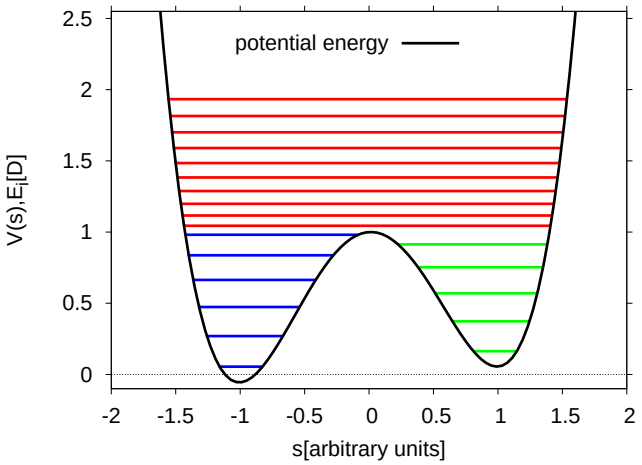

FIG. 1. Potential energy curve and energy eigenvalues in the left well (blue), in the right well (green), and over the barrier (red) for the input parameters $d = 1$, $a_4 = 1D$, $a_1 = 5.5 \cdot 10^{-2} D$, and $I = 1.62 \cdot 10^2 \hbar^2 D^{-1}$. The cutoff is set to twice the barrier height D.

The interaction with the electric field $u(t)$ is simplified to the semiclassical dipole approximation $-\mu u(t)$. The transition dipole moments are calculated from the energy eigenfunctions assuming a dipole moment operator linear in s with unit slope: $\mu = s$. In addition to the potential energy curve, the structure of the equations of motion, the positivity of the populations, and the occurrence of a simple zero eigenvalue form a common ground with the semi-discretized Fokker-Planck equation model under investigation in Ref.[41]. However, the used basis sets, on one side a spatial basis and on the other side the basis of energy eigenstates, are one of the differences between the classical and quantum mechanical model systems.

Concerning the observables of the system, we investigate how much population is localized in the left well and the right well, and which part is delocalized over the barrier. The corresponding observability matrix $C \in \mathbb{R}^{3\times 441}$

is given by:

$$C_{1,k} = \sum_{j=1}^{6} \delta_{k,2j-1} \qquad \text{left well}$$

$$C_{2,k} = \sum_{j=1}^{5} \delta_{k,2j} \qquad \text{right well}$$

$$C_{3,k} = \sum_{j=1}^{10} \delta_{k,11+j} \qquad \text{delocalized}$$

For the complete description of the system, another two parameters have to be set: The energy equivalent of temperature T, $\beta^{-1} = k_B T$, and the dissipative transition rate $\Gamma_{2\to 0}$ (due to wave function overlap the reference quantity should rather be $\Gamma_{2\to 0}$ than $\Gamma_{1\to 0}$). In addition, for the consideration of the dynamics of the system, the control field $u(t) = u_0 \cos(\Omega t - \varphi_0) b(t)$ with the initial phase φ_0 and the shape function $0 \leq b(t) \leq 1$ has to be determined. In order to relate these quantities to energy differences which characterize the potential curve we introduce the following dimensionless variables for the temperature $\theta = k_B T/(\hbar\omega_{2,0})$, for the dissipative transition rate $\zeta = \Gamma_{2\to 0}/\omega_{2,0}$, and for the control field $\xi = \mu_{2,0} u_0/\omega_{2,0}$ with the Bohr frequency $\omega_{2,0} = 0.2148 D\hbar^{-1}$ and the transition dipole moment $\mu_{2,0} = 0.1189 e a_0 \hbar^{-1}$.

B. Example 1: High temperature, fast relaxation

Setting the value $k_B T = D$ (i. e. $\theta = 4.655$) reflects a system at fairly high temperature. Subsequently all states are populated notably in the equilibrium, even the delocalized states lying over the barrier. For the equilibrium distribution, determined by Eq. (11), population of the lowest state in the left well is $\rho^e_{0,0} = 0.10449$ whereas the population of the highest delocalized state is given by $\rho^e_{20,20} = 0.01597$. The populations in the left well sum up to $y_1(0) = 0.40356$, in the right well the corresponding observable is $y_2(0) = 0.32838$, and the delocalized states lying over the barrier exhibit a total population of $y_3(0) = 0.26806$. The dissipative transition rate $\Gamma_{2\to 0} = D\hbar^{-1}$ (i. e. $\zeta = 4.655$) causes a fast relaxation of non-equilibrium states.

As a first step we have a closer look at matrix A (structured like Eq. (A2) in Appendix A) describing the field-free quantum dynamics and its eigenvalue spectrum. The most interesting part is the first, real valued full block of the block diagonal matrix A. It represents the dissipative coupling among populations and is displayed in Figure 2. It consists of the rates $\Gamma_{m\to n}$ for the off-diagonal elements and the total transition rates for the diagonal elements. The even-odd alternations for $m, n < 10$ simply reflects the extremely low overlap between states in the left and the right well. Diagonalization of the first block of A can easily be performed and leads to real eigenvalues. Due to Eqs. (6) and (A2) the second, the diagonal block of A

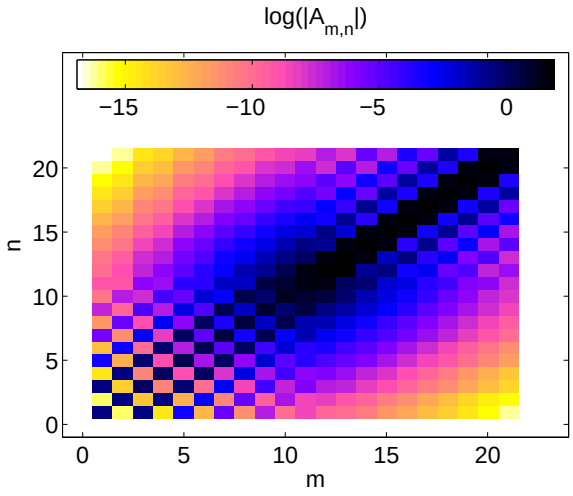

FIG. 2. Example 1: Logarithmic plot of the upper diagonal block of A which consists of the sum of dissipative reaction rates matrix Γ and the total transition rates.

which represents the dynamics of the coherences exhibits a simple structure: The real part is solely determined by the dephasing rates $\gamma_{m,n}$ whereas the imaginary part of the diagonal elements of A represents the negative Bohr frequencies.

Next we perform the balancing transformation which results in the Hankel singular values displayed in Figure 3 (together with those for the following two examples). The descent of the HSVs can be roughly characterized as follows: The first fifty HSVs decrease exponentially by about seven orders of magnitude. After that, the decrease flattens to a exponential decrease of another seven orders of magnitude between $i = 100$ and $i = 315$.

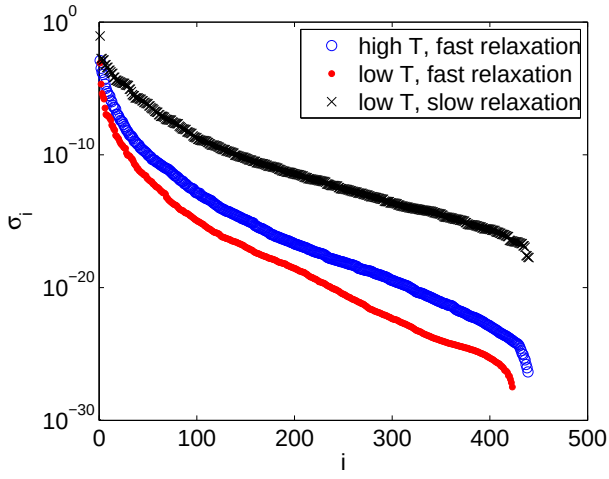

FIG. 3. The diagonal elements of Σ, also referred to as Hankel singular values for high temperature and fast relaxation (example 1, blue circles), low temperature and fast relaxation (example 2, filled red circles), and low temperature and slow relaxation (example 3, black crosses)

In the remainder of this work we assess the quality of the balanced truncation method by comparing the reference output $y(t) = (y_1(t), y_2(t), y_3(t))^T$ with the balanced, truncated (to r modes), and backtransformed output $y^{(r)}(t) = CT^{(r)}(T^{-1})^{(r)}x(t)$, where $(T^{-1})^{(r)}$ is the truncated $r \times n$ matrix of the balancing transform, $T^{(r)}$ is the truncated $n \times r$ matrix of its inverse (see Figure 4), and $z^{(r)}(t) = T^{-1})^{(r)}x(t)$ are the balanced and truncated (to r components) density matrix elements. Initially, we have $y(t = 0) = y_e = Cx_e$. Because we transform to the eigenstate basis of A and split off the stationary state before balancing, reference output at time zero can always be reproduced, regardless of the number of truncated modes. This is due to the fact the we always consider the equilibrium density whereas truncation acts on its orthogonal complement, see Section B. In contrast, using a shift of $A \to A - \alpha I$ in order to eliminate the zero eigenvalue of A, unphysical populations are produced if the number r of remaining balanced density matrix elements is too small. For this reason we concentrate on the case of splitting off the stationary state.

Next, we consider the field driven dynamics for $t > 0$. Due to the fast relaxation and the high temperature, we use a simple non-oscillating sinusoidal half cycle pulse $u(t) = u_0 \sin(\Omega t)$, $\Omega = 0.196\, D\hbar^{-1}$, $0 \le t \le \pi/\Omega$, $u_0 = 7.5\, De^{-1}a_0^{-1}$. With $\omega_{2,0} = 0.2148 D\hbar^{-1}$ and $\mu_{2,0} = 0.1189 e a_0 \hbar^{-1}$, the dimensionless parameter ξ can be determined to $\xi = 4.1515$. We want to observe how the populations of localized states in the left well, in the right well, and of delocalized states over the barrier of the potential energy curve evolve and relax for the time intervall $0 \le t \le 3\pi/\Omega$. At time $t = 0$ the system is in equilibrium. The control field serves to populate the states over the barrier and to transfer population between left and right well.

As a quantitative measure for the quality of balanced truncation approximation, we monitor the relative root mean square (rms) deviations $\|y^{(r)} - y\|_2 / \|y - y_e\|_2$ of the output integrated over time. The time evolution of the control target y for x starting from $x_0 = 0$ (cf. Figure 4) shows for a truncation to $r = 5$ a relative rms deviation between 6.71% for the right well and 9.70% for the left well with the mean value of 8.65% for all populations (cf. Table I) compared to the propagated original system, which is a surprisingly good result for only five components of z and diminishes the number of density matrix elements by a factor 88. In general, deviations get even smaller with increasing r: For $r = 10$, the rms deviations are spread between 1.22% for the delocalized states and 5.08% for the states in the right well, for all states we find 2.01% mismatch. Finally, for $r = 20$ the relative rms deviations are about 1%.

A closer look at the coefficients of the balancing transform reveals, that the five highest HSVs are characterized by populations of the left well (σ_1), coherences between neighboring states in the left well (σ_2, σ_5), and populations of the right well (σ_3, σ_4). Results for $r = 10$ are better since populations of levels near the barrier (σ_6, σ_{10}),

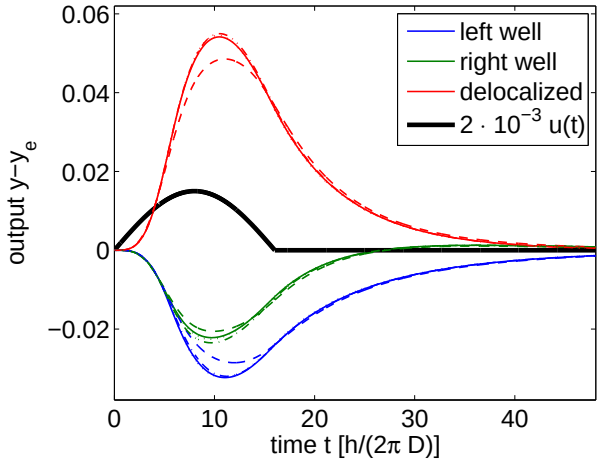

FIG. 4. Example 1: Deviation of population from equilibrium for states localized in the left (blue) , and in the right well (green), and delocalized states over the barrier (red) as a function of time for $r = 5$ (dashed), $r = 10$ (dashed-dotted) and $r = 20$ (dotted lines). The solid colored lines mark the untruncated case, and the solid black line is the control field.

TABLE I. Relative root mean square deviations (rms) between truncated (to r remaining elements of z) and untruncated dynamics of shifted populations for high temperature and fast relaxation (example 1)

r	left well	right well	delocalized	all
5	9.70%	6.71%	8.45%	8.65%
10	1.53%	5.08%	1.22%	2.01%
20	0.88%	1.31%	0.87%	0.92%

and coherences between neighboring states in the right well (σ_9) and around the barrier (σ_7) are included. That means that the balancing transform builds up balancing states with the highest HSVs from linear combinations of density matrix elements of similar type (e. g. populations of the right well). If all important informations are included full dynamics will be simulated properly by the truncated setting. In general, however, the linear combinations are neither intuitive nor representing an ascending or descending order of energy values. We hope that future considerations (e. g., in the Floquet picture) will reveal this situation.

C. Example 2: Low temperature, fast relaxation

In the following we consider the case of lower temperature. The temperature equivalent of the energy, $k_B T = 0.1D$, which is about the energy level splitting ($\theta = 0.4655$) leads to an equilibrium population of the lowest level in the left well of $\rho^e_{0,0} = 0.65771$ and the lowest level in the right well exhibits a population of $\rho^e_{1,1} = 0.22182$. The total populations of left and right

well are given by $y_1(0) = 0.74630$ and $y_2(0) = 0.25364$, respectively, whereas the total population over the barrier can be neglected ($y_3(0) = 6.1257 \cdot 10^{-5}$). Due to the low temperature, oscillating pulses can be used to efficiently transfer population and we chose a pulse which extends over three periods with a sine squared envelope: $u(t) = u_0 \cos(\Omega t) \sin^2\left(\frac{\pi t}{t_f}\right)$, $u_0 = 3.75 De^{-1} a_0^{-1}$, $\xi = 2.0758$, $\Omega = 0.196 D\hbar^{-1}$, $0 \le t \le t_f = 100\,\hbar D^{-1}$. The control field amplitude was adjusted in order to provide population transfer similar to the first example. The combination of fast relaxation and low temperature effects that population which is transferred from the left well to the delocalized states over the barrier are depopulated immediately for the benefit of the states in the right well. Consequently, no population tranfer between the wells occurs after the control field excitation has sufficiently died out toward the end of the pulse (cf. Figure 5).

Although the decrease of the HSVs is slightly faster than in the first example, see Figure 3, in this case more balanced states are needed to reproduce the reference propagation with a sufficient quality. Below $r = 21$ populations in the delocalized states over the barrier behave unphysical. For $r = 21$, the relative rms deviation is about 11% for the both wells. The high relative (94.14%) but small absolute deviation for the delocalized states over the barrier hardly influence the total deviation (11.31%, see also Table II) which is a consequence of the almost unpopulated delocalized states at all times. For $r = 29$ the rms mismatch is about 4% in the wells and 18.58% for the delocalized states. If we increase the number of remaining components of z step by step in the range between $r = 20$ and $r = 50$ we recognize oscillations of the rms mismatch in each part of the potential as a function of r. The deviations, both in the wells, and in all states turn below 1% for $r = 40$. For the same reasons, as mentioned above, rms mismatch for the delocalized states is higher (9.56%) but decreases for increasing r. It can be seen from the coefficients of the balancing transformation that the coherences between neighboring states inside the wells don't play a dominant role. Decreasing the control field to $u_0 = 1.5 De^{-1} a_0^{-1}$, $\xi = 0.8303$ improves the rms mismatch of all populations to 10% if $r = 9$ which turns below 1% if r increases to 24. By conducting additional tests for all other examples we could verify that in general r has to be increased if one is interested in obtaining the same accuracy of model reduction using higher field energies.

D. Example 3: Low temperature, slow relaxation

In a third example we consider the same low temperature ($\theta = 0.4655$) as in example 2 but we add the possibility to analyze the depopulation of the delocalized states. Therefore, we chose slow relaxation by setting the dissipative transition rate to $\Gamma_{2\to 0} = 10^{-3}\, D\hbar^{-1}$

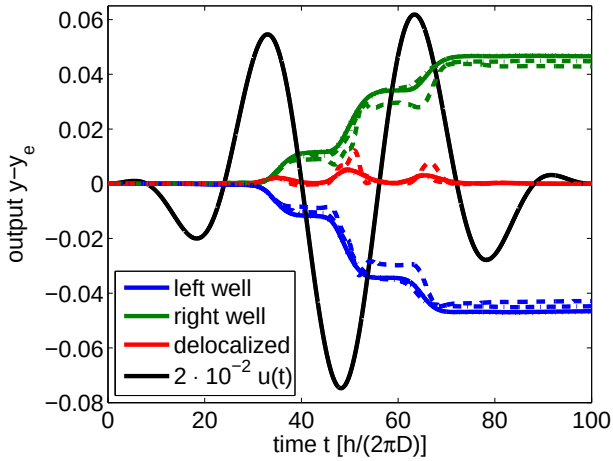

FIG. 5. Example 2: Population (with respect to equilibrium population) of states localized in the left (blue) , and in the right well (green), and delocalized states over the barrier (red) as a function of time for $r = 21$ (dashed), $r = 29$ (dashed-dotted), and $r = 40$ (dotted lines). The solid line marks the untruncated case.

TABLE II. Relative root mean square deviations between truncated (to r remaining components of z) and untruncated dynamics of shifted populations for low temperature and fast relaxation (example 2)

r	left well	right well	delocalized	all
21	10.24%	11.56%	94.14%	11.31%
29	4.19%	4.14%	18.58%	4.21%
40	0.70%	0.71%	9.56%	0.77%

which leads to $\zeta = 4.655 \cdot 10^{-3}$. The control field is described by the function given in the preceeding example. While Ω takes the same value, the other constants are changed: $u_0 = 0.2\, De^{-1} a_0^{-1}$, $t_f = 360\,\hbar D^{-1}$, and therefore $\xi = 0.1107$. Consequently the pulse extends over 11 periods which is depicted in Fig. 6. The HSVs decrease more slowly than in the examples discussed before, see Figure 3.

In contrast to example 2, populations of the delocalized states grow at the expense of the major fraction of the population in the left well and the minor fraction of the population in the right well. Only toward the end of the control pulse, when the amplitude of the exciting pulse has dropped down sufficiently, relaxation becomes visible and depopulates the states lying over the barrier for the benefit of the states in the right well (major part) and left well (minor part, cf. Fig. 6).

For $r = 60$ the time-dependent output shows the correct trend, but deviations are enormous (see Table III). For $r = 90$ the result is already quite good for left well (rms=6.56%) and the delocalized states over the barrier (rms=7.04%) whereas the right well still shows stronger deviations (rms=35.16%). The rms mismatch

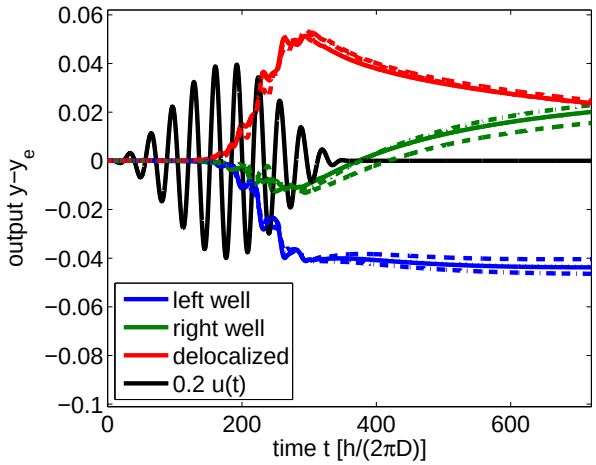

FIG. 6. Example 3: Population (with respect to equilibrium population) of states localized in the left (blue) , and in the right well (green), and delocalized states over the barrier (red) as a function of time. Dashed lines indicate a truncation to $r = 90$ states, dashed-dotted lines mean $r = 110$ and dotted lines label $r = 180$. The solid line marks the untruncated case.

of all populations is 10.22% . For $r = 110$ all relative rms-deviations shrink and the total rms deviation is 5.36%. In order to confine the mismatch below 1% $r = 180$ remaining elements of z are needed. In contrast to the preceeding examples, the coefficients of the balancing transform show more state specific behavior and only few population dominated eigenvectors for the first 60 HSVs.

TABLE III. Relative root mean square deviation of the output integrated over time for truncated (to r remaining components of z) with respect to untruncated dynamics of shifted populations for low temperature and slow relaxation (example 3)

r	left well	right well	delocalized	all
60	45.81%	48.05%	66.38%	55.21%
90	6.56%	35.16%	7.04%	10.22%
110	4.86%	14.87%	3.50%	5.36%
180	0.58%	1.82%	0.72%	0.74%

V. CONCLUSIONS AND OUTLOOK

This paper represents a first application of balanced truncation to light-induced control of open quantum systems. This method efficiently reduces the dimensionality of the LvNE by constructing states which are controllable and observable at the same time. While originally developed for control problems of linear systems the bilinear nature of the system-field coupling necessitates the solution of generalized Lyapunov equations. In our application to a one-dimensional model problem for different temperatures and relaxation rates, the balanced truncation method has shown its great potential in simplifying quantum-dynamical simulations occuring in optimal control problems. In particular, the input-output behavior of the original system can be well approximated by drastically reduced systems. For a relative rms deviation of 5% in the output the dimensionality of the system can be reduced by about 98% for high temperature and fast relaxation (example 1), while for lower temperatures a reduction of 94% or 76% can be achieved for faster (example 2) or slower relaxations (example 3), respectively. The differences in the degree of reduction can be partly attributed to the different decay of the Hankel singular values of controllability and observability Gramians which is the foundation of the theory of balanced truncation method for linear systems. Also for the bilinear system considered in the present work, the overall behavior is a decrease of the error with rising r, the dimensionality of the reduced model. A drawback compared to balanced truncation for linear systems is the non-monotonic behavior of the error as a function of r. However, the location of a local minimum of the error is independent of the external field amplitude. In contrast, the truncated dimensionality r needed to obtain a given accuracy for the output dynamics rises with the field amplitude.

In future work, the dependence of the accuracy of balanced truncated systems on the dimensionless parameters representing temperature θ, dissipative transition rate ζ, and control field amplitude ξ should be investigated systematically for real systems e. g. from atomic or molecular physics. Furthermore, it would be interesting to study the effect of different control targets expressed by different observability matrices C for given controllability. Especially the sensitivity of the required dimensionality r to achieve a desired accuracy on the nature of matrix C should be properly examined. In particular, the rather coarse grained target of population transfer between the wells of the model potential considered in section IV could be replaced by finer details like state selective control targets. Our first test calculations have shown that these goals are within reach. Finally, the relation between PCA and balanced truncation could be further explored. This would also allow to systematically impose further constraints on the truncation procedure e. g. positivity of the populations or even a Liouville-von Neumann structure of the reduced system.

Yet another possible advancement of the balanced truncation method could be a combination with the Floquet picture of photon dressed states. By eliminating the fast carrier frequencies the control problem for typical laser pulses could be reduced to an optimization of few parameters such as frequencies, intensities and pulse shape parameters[56,57].

ACKNOWLEDGMENTS

The authors thank the Deutsche Forschungsgemeinschaft for financial support in the framework of the Sonderforschungsbereich 450: "Analyse und Steuerung photoinduzierter ultraschneller Reaktionen" and the DFG-Forschungszentrum Matheon.

Appendix A: Vectorization of the density matrix

We will illustrate the procedure by means of a two state model ($q = 2$) and use the tetradic notation introduced by Mukamel[58]:

$$\rho = \begin{pmatrix} \rho_{0,0} & \rho_{0,1} \\ \rho_{1,0} & \rho_{1,1} \end{pmatrix} \mapsto x = \begin{pmatrix} \rho_{0,0} \\ \rho_{1,1} \\ \rho_{0,1} \\ \rho_{1,0} \end{pmatrix}, \tag{A1}$$

where the order of the matrix elements $\rho_{l,m}$ in the vector x is arbitrary but fixed. Here we start with all the populations and proceed with the coherences (i. e. the off-diagonal elements of the density matrices) leading to the expression:

$$A = \begin{pmatrix} \boxed{\begin{matrix} -\gamma_{0,0} & \Gamma_{1\to 0} \\ \Gamma_{0\to 1} & -\gamma_{1,1} \end{matrix}} & 0 \\ 0 & \boxed{\begin{matrix} -i\omega_{0,1} - \gamma_{0,1} & 0 \\ 0 & -i\omega_{1,0} - \gamma_{1,0} \end{matrix}} \end{pmatrix} \tag{A2}$$

and

$$N = \begin{pmatrix} 0 & & -\mu_{1,0} & \mu_{0,1} \\ & & \mu_{1,0} & -\mu_{0,1} \\ -\mu_{0,1} & \mu_{0,1} & \mu_{0,0} - \mu_{1,1} & 0 \\ \mu_{1,0} & -\mu_{1,0} & 0 & \mu_{1,1} - \mu_{0,0} \end{pmatrix} \tag{A3}$$

Note, that a generalization to $q > 2$ is straight forward.

The chosen order in the vectorization (A1) has the advantage, that A is blockdiagonal with block sizes q and $(n - q)$ where the latter block exhibits diagonal structure. The diagonal elements of A contain $-i\omega_{l,m} - \gamma_{l,m}$, i. e. differences of energy eigenvalues and total dephasing rates. Those off-diagonal elements of A which represent couplings of different populations include a corresponding dissipative transition rate. The elements of N represent the coupling between the external field $F(t)$ and the vectorized density $x(t)$ through susceptibility μ. Also the matrix N can be divided in submatrices of size $q \times q$, $q \times (n - q)$, $(n - q) \times q$, and $(n - q) \times (n - q)$. In contrast to A, the upper left $q \times q$ submatrix of N is the zero-matrix[47]. The off-diagonal ones contain off-diagonal matrix elements $\mu_{l,m}$ whereas the diagonal ones are differences of $\mu_{l,l}$.

For the observables given in (9), the vectorization (A1) provides:

$$C = \begin{pmatrix} O^{(1)}_{0,0} & O^{(1)}_{1,1} & O^{(1)}_{1,0} & O^{(1)}_{0,1} \\ O^{(2)}_{0,0} & O^{(2)}_{1,1} & O^{(2)}_{1,0} & O^{(2)}_{0,1} \end{pmatrix}. \tag{A4}$$

The shift is in the case of the two state model given by $x_e = (\rho^e_{0,0}, \rho^e_{1,1}, 0, 0)^T$, and leads to:

$$B = \begin{pmatrix} 0 \\ 0 \\ -\mu_{0,1} \\ \mu_{1,0} \end{pmatrix} (\rho^e_{0,0} - \rho^e_{1,1}). \tag{A5}$$

Appendix B: Solvability and numerical solution of the generalized Lyapunov equations

We shall briefly discuss the solution of the generalized Lyapunov equations (29). To this end recall that a system is called stable when the system matrix A has only eigenvalues in the open left half complex plane (i.e., excluding the imaginary axis). Stability thus means that there are constants $\lambda, a > 0$ such that $\|\exp(At)\| \leq \lambda \exp(-at)$ where $\|\cdot\|$ is any suitable matrix norm. If moreover

$$\frac{\lambda^2}{2a}\|N\|^2 < 1 \tag{B1}$$

then controllability and observability Gramians exist[46]. In contrast, for the solvability of the "ordinary" Lyapunov equations (16), stability is the only requirement. If moreover the pair (A, B) satisfies Kalman's rank condition

$$\operatorname{rank}(B|\, AB|\, A^2B|\, \ldots|\, A^{n-1}B) = n \tag{B2}$$

for the Kalman block matrix $(B|\, AB|\, A^2B|\, \ldots|\, A^{n-1}B) \in \mathbb{C}^{n\times np}$ then W_c is positive definite (complete controllability).[59] In turn, if the pair (A^*, C^*) satisfies the rank condition, then also W_o is positive definite (complete observability).

Direct methods for solving generalized Lyapunov equations have a numerical complexity $\mathcal{O}(n^6)$ which makes computing the Gramians a challenge even for medium-sized systems. For stable matrix A and for the controllability Gramian, one can resort to iterative schemes such as[60]

$$AX_{j+1} + X_{j+1}A^* = -NX_jN^* - BB^*, \quad X_0 = 0 \tag{B3}$$

which requires the solution of a standard Lyapunov equation in each step (the iteration for the observability Gramian follows analogously). Convergence $X_j \to W_c$ is guaranteed if the eigenvalue of A with the largest (negative) real part is sufficiently separated from the imaginary axis.[61]. In view of the solvability condition (B1), this can be obtained by either a suitable scaling $u \mapsto \eta u$,

$N \mapsto \eta^{-1}N$, $B \mapsto \eta^{-1}B$ with $\eta > 1$ that leaves the equations of motion invariant (but, clearly, not the Gramians), or by shifting $A \mapsto \alpha I$ with $\alpha > 0$ so as to further stabilize the system matrix A.[37,62]

By reducing the solution of the generalized Lyapunov equation to n_{it} solutions of an ordinary Lyapunov equation, the numerical complexity of the iterative scheme (B3) reduces to $\mathcal{O}(n_{it}n^3)$. For even larger systems ($n \approx 10^6$), also the iterative scheme may be impractical so that further pre-conditioning of the matrices A, B, N, C becomes necessary, e.g., by applying Krylov subspace methods[35–37] and/or by exploiting the sparsity of the matrices.

Finally, we want to remind that the advantage of using the balanced truncation procedure is based on the fact that the most time-consuming step has to be carried out only once while every single propagation of the LvNE is using the truncated system. An alternative to the solution of the Lyapunov equation is presented in the following.

Appendix C: Relation to Principical Component Analysis (PCA)

Here we want to show how balanced truncation is linked to the more common PCA[63–66], also referred to as proper orthogonal decomposition (POD)[67], which is another frequently used technique for model reduction. Moreover, as we shall demonstrate below, it offers a promising alternative to the solution of the generalized Lyapunov equations discussed in Appendix B. The balancing method admits an intriguing variational formulation. Consider the stochastic differential equation

$$dx(t) = Ax(t)dt + (Nx(t) + B)\, dw(t)\,, \quad x(0) = 0 \quad \text{(C1)}$$

of Itô type, i. e. the stochastic analogue of the deterministic bilinear system

$$\dot{x}(t) = (A + Nu(t))\, x(t) + Bu(t)\,, \quad x(0) = 0\,.$$

Here w denotes the one-dimensional standard Brownian motion. Suppose that $\{x(t_0), x(t_1), \ldots, x(t_M)\} \subset \mathbb{R}^n$ with $0 = t_0 < t_1 < \ldots < t_M = T$ is a discrete-time trajectory of (C1). We want to find the best approximating linear subspace $S \subset \mathbb{R}^n$ of dimension $k < n$ that minimizes the mean squared distance

$$D_M(Q) = \frac{1}{M}\sum_{i=0}^{M} \|x(t_i) - Qx(t_i)\|_G^2 \quad \text{(C2)}$$

of the trajectory from $S \subset \mathbb{R}^n$. Here $\|x\|_G = \sqrt{x^*Gx}$ is the Euclidean distance with respect to the (constant) metric tensor $G \in \mathbb{R}^{n\times n}$ and Q denotes a projection that is orthogonal with respect to this inner product, i.e., for which $Q^*G(I - Q) = 0$. Since moreover $Q^2 = Q$ for any projection, we have $\|x - Qx\|_G^2 = \|x\|_G^2 - \|Qx\|_G^2$ which implies that minimizing D_M is equivalent to maximizing the "energy" of the projection,

$$E_M(Q) = \frac{1}{M}\sum_{i=0}^{M} \|Qx(t_i)\|_G^2\,. \quad \text{(C3)}$$

Now we show that the k-dimensional subspace $S \subset \mathbb{R}^n$ that maximizes (C3) is spanned by the dominant k eigenvectors of the generalized eigenvalue problem

$$C_M G\, v = \lambda v\,, \quad \text{(C4)}$$

where C_M is the empirical covariance matrix

$$C_M = \frac{1}{M}\sum_{i=0}^{M} x(t_i)x(t_i)^* \quad \text{(C5)}$$

of the data. Without loss of generality we may consider the case $k = 1$. In other words, we seek the best-approximating one-dimensional subspace for our data. To this end let $w \in \mathbb{R}^n$ denote the vector spanning this subspace, i.e., $S = \mathrm{span}\{w\}$. Assuming that w is normalized, $\|w\|_G = 1$, the projection Q must be of the form

$$Qx = \langle w, x\rangle_G\, w\,.$$

Inserting the last expression into E_M, our least squares problem turns out to be

$$\max_w \frac{1}{M}\sum_{i=0}^{M} \langle w, x_i\rangle_G^2 \quad \text{s.t.} \quad \langle w, w\rangle_G = 1\,. \quad \text{(C6)}$$

Defining the functional

$$L(w) = \frac{1}{M}\sum_{i=0}^{M} \langle w, x_i\rangle_G^2 - \lambda\,(\langle w, w\rangle_G - 1) \quad \text{(C7)}$$

a necessary condition for (C6) is that $\delta L(w) = 0$ which reads

$$\frac{1}{M}\sum_{i=0}^{M} x_i\, \langle w, x_i\rangle_G = \lambda w\,.$$

The last equation can be recast as

$$\left(\frac{1}{M}\sum_{i=0}^{M} x_i x_i^*\right) Gw = \lambda w\,,$$

which is nothing but the generalized eigenvalue problem (C4). Iterating the argument with $S = \mathrm{span}\{w_1, w_2\}$ where $w_1 = w$ and $\langle w_2, w\rangle_G = 0$ and so on and so forth yields that the solution of the least squares problem (C2) is obtained by projecting the data $\{x_0, x_1, \ldots, x_M\} \subset \mathbb{R}^n$ onto the first k eigenvectors of

$$C_M G w = \lambda w$$

with

$$C_M = \left(\frac{1}{M} \sum_{i=0}^{M} x_i x_i^* \right)$$

being the unbiased estimator of the covariance matrix of the data.

Clearly, when $C_M = W_c$ is the controllability Gramian and $G = W_o$ is the observability Gramian, then (up to scaling) the eigenvectors of (C4) essentially yield the balancing transformation (25).

We will now argue that C_M for $M \to \infty$, $t_M \to \infty$, the asymptotic empirical covariance matrix, converges to the controllability Gramian W_c. Thus, solving the least-squares problem (C2) with respect to the observability metric $G = W_o$ is in indeed equivalent to balancing (under the assumption that W_o is positive definite). To see this, it is helpful to note that $\langle x(t) \rangle = 0$ when $x(0) = 0$, for the increments dw of the Brownian motion are centered Gaussian random variables. (We use the notation $\langle \cdot \rangle$ to denote the expectation over the all realizations of w.) Then, using Itô's formula, it follows[68]

$$\begin{aligned} d\left(x(t)x(t)^*\right) &= x(t)dx(t)^* + dx(t)\,x(t)^* \\ &\quad + \left(Nx(t) + B\right)\left(Nx(t) + B\right)^* dt\,. \end{aligned}$$

We define $\mathcal{C}(t) = \langle x(t)x(t)^* \rangle$ to be the covariance matrix of x at time t. Inserting (C1) in the last equation, taking the expectation, and interchanging the expectation with the differentiation, it follows that S solves

$$\dot{\mathcal{C}}(t) = A\mathcal{C}(t) + \mathcal{C}(t)A^* + N\mathcal{C}(t)N^* + BB^*\,. \qquad \text{(C8)}$$

The solvability condition (B1) for the generalized controllability Gramian, i.e., for the matrices A, B, N guarantees that $\dot{\mathcal{C}} \to 0$ as $t \to \infty$ which entails[69]

$$W_c = \lim_{t \to \infty} \mathcal{C}(t)\,.$$

Therefore also $C_M \to W_c$ as $M \to \infty$ which clearly remains true if $N = 0$, i.e., when the system is linear.[41] The observability Gramian can be computed analogously. To sum up, we have proved that solving the least-squares problem (C2) with $G = W_o$ is equivalent to balanced truncation when the deterministic control u in either (14) or (26) is replaced by Gaussian white noise dw/dt. Hence, the method of PCA lends itself as an alternative to the (expensive) solution of the generalized Lyapunov equations (see Appendix B) for calculating the controllability and observability Gramians[41].

[1] S. A. Rice and M. Zhao, *Optical Control of Molecular Dynamics* (Wiley & Sons, New York, 2000)
[2] M. Shapiro and P. Brumer, *Principles of Quantum Control of Molecular Processes* (John Wiley & Sons, 2003)
[3] V. Sundström, ed., *Femtochemistry and Femtobiology: Ultrafast Reaction Dynamics at Atomic Scale Resolution*, Nobel symposium, Vol. 101 (Imperial College Press, London, 1997)
[4] O. Kühn and L. Wöste, eds., *Analysis and Control of Ultrafast Photoinduced Reactions* (Springer, Berlin, 2007)
[5] M. Shapiro and P. Brumer, J. Chem. Phys. **84**, 4103 (1986)
[6] D. J. Tannor, R. Kosloff, and S. A. Rice, J. Chem. Phys. **85**, 5805 (1986)
[7] A. P. Peirce and M. A. Dahleh, Phys. Rev. A **37**, 4950 (1988)
[8] A. H. Zewail, *Femtochemistry: Ultrafast Dynamics of the Chemical Bond* (World Scientific, Singapore, 1994)
[9] J. Manz and L. Wöste, eds., *Femtosecond Chemistry*, 2nd ed. (WILEY-VCH Verlag, Weinheim, 1995)
[10] V. Bonačić-Koutecký and R. Mitrić, Chem. Rev. **105**, 11 (2005)
[11] R. Kosloff, S. Rice, P. Gaspard, S. Tersigni, and D. Tannor, Chem. Phys. **139**, 201 (1989)
[12] D. J. Tannor and V. A. Kazakov, in *Time-Dependent Quantum Molecular Dynamics*, edited by J. Broeckhove and L. Lathouwers, NATO Advanced Research Workshop (Plenum, New York, 1992) pp. 347–360
[13] R. Judson and H. Rabitz, Phys. Rev. Lett. **68**, 1500 (1992)
[14] W. S. Warren, H. Rabitz, and M. Dahleh, Science **259**, 1581 (1993)
[15] W. Zhu, J. Botina, and H. Rabitz, J. Chem. Phys. **108**, 1953 (1998)
[16] U. Weiß, *Quantum dissipative systems*, Series in Modern Condensed Matter Physics, Vol. 10 (World Scientific, Singapore, 1999)
[17] V. May and O. Kühn, in *Charge and Energy Transfer Dynamics in Molecular Systems* (WILEY-VCH Verlag, 2004) pp. 81–194
[18] T. Gerdts and U. Manthe, J. Chem. Phys. **106**, 3017 (1997)
[19] A. Raab, I. Burghardt, and H.-D. Meyer, J. Chem. Phys. **111**, 8759 (1999)
[20] H.-D. Meyer and G. A. Worth, Theor. Chem. Acc. **109**, 251 (2003)
[21] M. Nest and H.-D. Meyer, J. Chem. Phys. **119**, 24 (2003)
[22] B. Wolfseder and W. Domcke, Chem. Phys. Lett. **235**, 370 (1995)
[23] H.-P. Breuer, W. Huber, and F. Petruccione, Comp. Phys. Comm. **104**, 46 (1997)
[24] M. Khasin and R. Kosloff, Phys. Rev. A **78**, 012321 (2008)
[25] G. Füchsel, T. Klamroth, J. C. Tremblay, and P. Saalfrank, Phys. Chem. Chem. Phys. **12**, 14082 (2010)
[26] C. Mullis and R. Roberts, IEEE Trans. Circuits Syst. **23**, 551 (1976)
[27] B. Moore, IEEE Trans. Automat. Control **AC-26**, 17 (1981)
[28] K. Glover, Int. J. Control **39**, 1115 (1984)
[29] Y. Liu and B. Anderson, Int. J. Control **50**, 1379 (1989)
[30] S. Gugercin and A. Antoulas, Int. J. Control **77**, 748 (2004)
[31] T. Reis and E. Virnik, SIAM J. Control Optim. **48**, 2600 (2009)
[32] C. Hartmann, V.-M. Vulcanov, and C. Schütte, Mult. Mod. Sim. **8**, 1348 (2010)
[33] C. Hartmann, "Balanced model reduction of partially-observed Langevin processes: an averaging principle," Submitted to: Math. Comput. Model. Dyn. Syst. (12.01.2010), http://publications.mi.fu-berlin.de/802/
[34] C. Hartmann, in *Proceedings of MATHMOD 09*, ARGESIM Report, Vol. 35, edited by I.Troch and F. Breitenecker (2009) pp. 1244–1255
[35] Z. Bai, Appl. Numer. Math. **43**, 9 (2002)
[36] Z. Bai and D. Skoogh, Linear Algebra Appl. **415**, 406 (2006)
[37] P. Benner and T. Damm, "Lyapunov equations, energy functionals, and model order reduction," Submitted to: SIAM J. Control Optim. (2009), http://www-user.tu-chemnitz.de/~benner/pub/BennerDamm_SICON2009.pdf
[38] L. Zhang and J. Lam, Automatica **38**, 205 (2002)
[39] M. Ottobre and G. A. Pavliotis, Nonlinearity **24**, 1629 (2011)
[40] Z. Ma, C. W. Rowley, and G. Tadmor, IEEE Trans. Automat. Control **55**, 469 (2010)
[41] C. Hartmann, A. Zueva, and B. Schäfer-Bung, "Balanced model reduction of bilinear systems with applications to positive systems," Submitted to: SIAM J. Control Optim. (28.05.2010), http://publications.mi.fu-berlin.de/911/
[42] H.-P. Breuer and F. Petruccione, *The theory of open quantum systems* (Oxford University Press, Oxford, 2002)
[43] G. Lindblad, Comm. Math. Phys. **48**, 119 (1976)
[44] M. Nest and P. Saalfrank, Chem. Phys. **268**, 65 (2001)

[45] I. Andrianov and P. Saalfrank, J. Chem. Phys. **124**, 034710 (2006)
[46] W. Gray and J. Mesko, in *Preprints of the 4th IFAC Nonlinear Control Systems Design Symposium* (Enschede, Netherlands, 1998) pp. 103–108
[47] S. W. Greenwald, *Local Dimension Reduction of a Dissipative Quantum Control System*, Diploma thesis, Freie Universität Berlin (2008)
[48] J. M. A. Scherpen, Syst. Control Lett. **21**, 143 (1993)
[49] A. Antoulas, *Approximation of Large-Scale Dynamical Systems* (SIAM, Philadelphia, 2005)
[50] Strictly speaking the term *transfer function* refers to the input-output map $y(u; x_0 = 0)$ in the frequency domain (i.e., in Fourier space) rather than in the time domain, but we will ignore this subtlety for the time being.
[51] S. Beyvers and P. Saalfrank, J. Chem. Phys. **128**, 074104 (2008)
[52] A. Isidori, IEEE Trans. Autom. Control **18**, 626 (1973)
[53] C. W. Rowley, Int. J. Bifurcat. Chaos **15**, 997 (2005)
[54] R. Meyer, J. Chem. Phys. **52**, 2053 (1970)
[55] C. C. Marston and G. G. Balint-Kurti, J. Chem. Phys. **91**, 3571 (1989)
[56] K. Drese and M. Holthaus, Eur. Phys. J. D **5**, 119 (1999)
[57] I. Horenko, B. Schmidt, and C. Schütte, J. Chem. Phys **115**, 5733 (2001)
[58] S. Mukamel, *Principles of nonlinear optical spectroscopy* (Oxford University Press, New York, 1995)
[59] H. Schneider, Numer. Math. **7**, 11 (1965)
[60] E. Wachspress, Appl. Math. Lett. **1**, 87 (1988)
[61] T. Damm, Numer. Linear Algebra Appl. **15**, 853 (2008)
[62] M. Condon and R. Ivanov, Int. J. Comp. Math. **24**, 202 (2005)
[63] T. Ichiye and M. Karplus, Proteins **11**, 205 (1991)
[64] A. Amadei, A. B. Linssen, and H. J. Berendsen, Proteins **17**, 412 (1993)
[65] S. Lall, J. E. Marsden, and S. Glavaški, Int. J. Robust Nonlin. Control **12**, 519 (2002)
[66] O. F. Lange and H. Grubmüller, Proteins **62**, 1053 (2006)
[67] P. Holmes, J. Lumley, and G. Berkooz, *Turbulence, Coherent Structures, Dynamical Systems and Symmetry* (Cambridge University Press, 1996)
[68] B. Øksendal, *Stochastic differential equations: an introduction with applications* (Springer, Berlin, 2003)
[69] T. Damm, *Rational Matrix Equations in Stochastic Control*, LNICS, Vol. 297 (Springer, 2004)